A cytological approach to study meiotic recombination and chromosome dynamics of Arabidopsis thaliana male meiocytes in three dimensions

Hurel, Aurélie; Phillips, Dylan; Vrielynck, Nathalie; Mézard , Christine; Grelon, Mathilde; Christophorou, Nicolas

Published in:
Plant Journal

DOI:
10.1111/tpj.13942

Publication date:
2018

Citation for published version (APA):
Hurel, A., Phillips, D., Vrielynck, N., Mézard , C., Grelon, M., & Christophorou, N. (2018). A cytological approach to study meiotic recombination and chromosome dynamics of Arabidopsis thaliana male meiocytes in three dimensions. *Plant Journal*, *95*(2), 385-396. https://doi.org/10.1111/tpj.13942

A cytological approach to study meiotic recombination and chromosome dynamics of *Arabidopsis thaliana* male meiocytes in three dimensions

Aurélie Hurel[1], Dylan Phillips[2], Nathalie Vrielynck[1], Christine Mézard[1], Mathilde Grelon[1*] and Nicolas Christophorou[1*]

1: Institut Jean-Pierre Bourgin, INRA, AgroParisTech, CNRS, Université Paris-Saclay, RD10, 78026 Versailles Cedex, France

2: Institute of Biological, Environmental and Rural Sciences (IBERS), Aberystwyth University, Penglais, Aberystwyth, Ceredigion, SY23 3DA, United Kingdom
*Corresponding authors: mathilde.grelon@inra.fr and nicolas.christophorou@inra.fr
Keywords: meiosis, *Arabidopsis thaliana*, 3D, telomere bouquet, synapsis initiation centers, chromosome dynamics.

ABSTRACT
During meiotic prophase I chromosomes undergo dramatic conformational changes that accompany chromosome condensation, pairing and recombination between homologs. These changes include the anchoring of telomeres to the nuclear envelope and their clustering to form a bouquet. In plants, these events have been studied and illustrated in intact meiocytes of large genome species. *Arabidopsis thaliana* is an excellent genetic model where major molecular pathways that control synapsis and recombination between homologs have been uncovered. Yet the study of chromosome dynamics is hampered by current cytological methods that disrupt the 3D architecture of the nucleus. Here we set up a protocol to preserve the 3D configuration of *A. thaliana* meiocytes. We showed that this technique is compatible with the use of a variety of antibodies that label structural and recombination proteins and were able to highlight the presence of clustered synapsis initiation centers at the nuclear periphery. By using fluorescence *in situ hybridization* (FISH) we also studied chromosome behavior during premeiotic G2 and prophase I, revealing the existence of a telomere bouquet during *A. thaliana* male meiosis. In addition we showed that the number of telomeres in a bouquet and its volume vary greatly thus revealing the complexity of telomere behavior during meiotic prophase I. Finally, by using probes that label subtelomeric regions of individual chromosomes we revealed differential localization behaviors of chromosome ends. Our protocol opens new areas of research to investigate chromosome dynamics in *A. thaliana* meiocytes.

INTRODUCTION
Meiosis is a cell division process common to all sexual eukaryotes. Following DNA replication, two rounds of chromosome segregation occur leading to the generation of haploid cells. During the first round (meiosis I), homologous chromosomes segregate thus reducing cell ploidy. During the second round (meiosis II), a mitosis-like division will occur where sister chromatids separate.
Proper chromosome segregation at anaphase I requires that during prophase I chromosomes encounter and recombine with their homologs (Zickler and Kleckner, 1999; Zickler, 2006; Mercier *et al.*, 2015; Zickler and Kleckner, 2015) which is accompanied by several well described events that structurally modify the chromosomes. Upon entry into prophase I at leptotene, chromosomes start to condense and are organized as arrays of chromatin loops along an axis composed of condensins, cohesins and axial proteins (Zickler and Kleckner, 1998). Concomitantly, meiotic recombination is initiated by the occurrence of double strand breaks (DSBs) on the chromosomes. A large proportion of these DSBs will be repaired using the homologous chromosome as a template, allowing their alignment. The ongoing DSB repair between homologous chromosomes by the recombination machinery is a prerequisite to the launching of the polymerisation of the synaptonemal complex (synapsis), defining the zygotene stage. At pachytene, synapsis is complete and meiotic recombination has resulted in the formation of crossovers (COs) that maintain homologs together and non-crossovers (NCOs). At this stage chromosomes can be distinguished as condensed structures

called bivalents. At diplotene chromosomes decondense only to recondense at diakinesis until metaphase I when they align at the metaphase plate prior to the first meiotic division.
Regarding chromosome dynamics, other major events occur during meiotic prophase I that have been illustrated in several species. At leptotene telomeres attach to the nuclear envelope (Klutstein and Cooper, 2014). Chromosome movements then take place the nature of which varies depending on the species studied. These movements are thought to facilitate homolog encounter, resolve chromosome entanglements and prevent ectopic recombination (Zickler and Kleckner, 2015). Finally another relatively conserved feature occurring during leptotene-zygotene stages concerns the clustering of chromosome ends at one side of the nucleus in a configuration called the "telomere bouquet" (Scherthan, 2001; Zickler and Kleckner, 1998). It was long thought that clustering of telomeres in a small volume would facilitate homology search (Scherthan, 2001). However, cytological and genetic data suggest that the bouquet has very little or no role in promoting pairing (Lee *et al.*, 2012; Zickler and Kleckner, 2016; Zickler, 2006). Rather, it is currently postulated that the bouquet would promote resolution of both chromosome entanglements and interactions between non-homologs (Zickler and Kleckner, 2016). The telomere bouquet has been clearly identified in barley, maize and rye, using protocols that preserve 3D organization of the meiocytes (Cowan and Cande, 2002; Carlton *et al.*, 2003; Phillips *et al.*, 2010; Phillips *et al.*, 2012; Murphy *et al.*, 2014) but *A. thaliana* has been, so far, considered an exception to the rule. Indeed, telomeres were shown to localize in one hemisphere of the nucleus but do not appear to display a clustered bouquet conformation like in the species listed above (Armstrong *et al.*, 2001; Roberts *et al.*, 2009; Varas *et al.*, 2015). However, chromosome behavior in these studies was investigated using spread meiocytes. Although the spreading technique presents numerous advantages, notably to allow the study of mechanisms that control synapsis and recombination, it is inappropriate for analyzing chromosome dynamics as the nuclear 3D
configuration is disrupted.
In order to investigate spatial chromosomal organisation all the way from premeiotic G2 until the end of meiosis, we developed a method to study meiosis in intact *A. thaliana* male meiocytes. We performed immunohistochemistry against various structural and recombination proteins at different stages of prophase I, showing that previously established cytological tools can be used with this approach. We also showed that this technique can be used to investigate chromosome dynamics by FISH. Using probes labelling either telomeric or subtelomeric regions, we revealed that *A. thaliana* meiocytes display a clear telomeric bouquet and that chromosome ends occupy different nuclear localization patterns. Overall our method allows the study of chromosome dynamics in intact *A. thaliana* male meiocytes. In combination with the powerful genetic resources available in that species, new areas of research can be envisaged to identify the factors that regulate chromosome dynamics and its function during meiotic prophase I in plants.

RESULTS and DISCUSSION

Development of the 3D protocol

Our protocol to maintain the *A. thaliana* meiocyte nuclei intact was adapted from the techniques used in various plants (Zheng *et al.*, 2014; Cowan and Cande, 2002; Phillips *et al.*, 2010; Murphy *et al.*, 2014) where meiocytes are maintained intact in a 5% polyacrylamide solution. The detailed protocol can be found in the Experimental procedures section. In brief, fresh *A. thaliana* anthers (0.35-0.45 mm to obtain meiocytes ranging from premeiotic interphase to pachytene) were harvested and fixed in 2% PFA for 20-30 minutes (Figure 1). While in other species anthers are then disrupted to extract the meiocytes before embedding in the acrylamide solution, this procedure proved to be more challenging in *A. thaliana* because of their small size. Instead, 10-15 intact anthers were directly embedded in a 10µl acrylamide drop on top of a coverslip (Figure 1). A second coverslip was placed on top of the anthers and slight pressure was applied with forceps on the coverslip to open the anthers and release the meiocytes (Figure 1). This step is crucial as excessive pressure will damage the meiocytes and their nuclear 3D configuration (see experimental procedures). Conversely, too little pressure will lead to insufficient release of material for analysis. After polymerization (around 30 minutes) the two coverslips are carefully separated with a razor blade and the fine layer of

polyacrylamide with the intact meiocytes remains on one of the coverlsips. After mounting with DAPI slides should be screened on the one hand to assay for the presence of meiocytes and their stages and on the other hand to monitor the integrity of meiocyte nuclei (see experimental procedures). Following these verification steps the meiocytes can then be subjected to immunohistochemistry or FISH. These procedures are very similar to the ones performed on spread meiocytes. Notably, antibody and probe dilutions as well as incubation times are unchanged. However, some technical adaptations due to the nature of the polyacrylamide gel were necessary (see experimental procedures for more details).

Identification of meiocytes during meiotic prophase I

Upon setting up the protocol, the first challenge was to identify the different stages of meiotic prophase I. For this we performed immunohistochemistry with the structural proteins ASY1 and ZYP1 (Higgins *et al.*, 2005) that respectively label the axial elements and the central element of the synaptonemal complex. ASY1 and ZYP1 dynamics have been extensively described on chromosome spread preparations (Armstrong *et al.*, 2002; Chelysheva *et al.*, 2007; Higgins *et al.*, 2005). Briefly, ASY1 appears as puncta during premeiotic G2 then makes continuous stretches in leptotene. At early zygotene ZYP1 appears as foci that define the synapsis initiation centers (SICs). During zygotene, ZYP1 becomes more continuous while ASY1 is not visible at synapsed regions. At pachytene ZYP1 localizes along the entire length of the bivalents. Using our 3D protocol, we could easily identify all the above described prophase I stages: premeiotic G2 nuclei with decondensed chromatin punctated ASY1 and no ZYP1 signal (Figure 2A; S1A). Leptotene nuclei with chromatin stretches colocalising with ASY1 that lacked ZYP1 (Figure 2B; S1B). Nuclei with either ZYP1 foci and/or with short ZYP1 stretches, indicating synapsis initiation, were identified as early zygotene stages (Figure 2C; S1C; Movie S1). We found that, as it has been described on spread chromosomes, the ASY1 signal is less detectable at the sites of ZYP1 loading (arrows in Figure 2C; S1C; Movie S1). Analyzing these early zygotene nuclei, we observed that the SICs are in their vast majority located at the nuclear periphery of the meiocytes (Figure 2C; S1C, S2A and Table S1). This trend is notably more obvious when we consider nuclei with few SICs, thereby representing the very early steps of synapsis. In that case, the proportion of peripherical SICs can be as high as 96.6% (Table S1, nuclei with less than 5 ZYP1 foci, n=13 nuclei). As the total number of SICs increases, the proportion of interstitial SICs also increases (S2B; Movie S2 and Table S1). This observation is reminiscent of what was described in plants with large genomes (maize, barley and wheat) where synapsis first occurs at sites at the nuclear periphery (Golubovskaya *et al.*, 2011; Higgins *et al.*, 2012; Khoo *et al.*, 2012; Barakate *et al.*, 2014; Colas *et al.*, 2017) but was unexpected given that *A. thaliana* short chromosomes are very differently structured (Künzel *et al.*, 2000; Giraut *et al.*, 2011; Roudier *et al.*, 2011; Mayer *et al.*, 2012; Sato *et al.*, 2012; Choulet *et al.*, 2014). We also noticed that in a significant number of nuclei the SICs located at the nuclear periphery had a tendency to cluster (44%, n=22; Figure 2C; Movie S1). As synapsis progresses, ZYP1 elongates along the chromosome axes and ASY1 becomes less detectable leading to a complementary pattern (Figure 2D; S1D; Movie S3). In addition, at sites where DAPI staining reveals pairing between chromosomes, the ZYP1 signal was always present (arrows in Figure 2E; S1E). At the end of zygotene, bivalents are clearly distinguishable and ZYP1 is present almost along their entire length (Figure 2F; S1F; Movie S4). At pachytene ZYP1 marks the entire length of the axis, except for a single ASY1 focus that persists and that presumably corresponds to the rDNA loci (arrow in Figure 2G; S1G). Thus, immunostaining with the structural proteins ASY1 and ZYP1 allowed us to identify the intact meiotic nuclei and characterize the different steps of meiotic prophase

Immunohistochemistry against meiotic recombination proteins on 3D preserved *A. thaliana* meiocytes

We performed immunohistochemistry against meiotic proteins that act at different steps of meiotic recombination to determine to what extent meiotic prophase I can be studied in intact meiocytes, and to compare their spatial and temporal patterns between intact and spread meiocytes. DMC1 is a recombinase that acts during double strand break (DSB) repair and was shown on spread meiocytes to be present as foci at recombination sites during leptotene and zygotene stages (Chelysheva *et al.*,

2007). In barley, where the investigations were performed on 3D meiocytes, a polarized pattern of DMC1 labelling was described, with the DMC1 foci first appearing at G2/leptotene on chromosomal distal regions and becoming interstitial only while meiosis progressed in leptotene (Higgins *et al.*, 2012). Here we found that DMC1 immunohistochemistry in intact *Arabidopsis* meiocytes recapitulates very well the observations made on spread meiocytes, with DMC1 foci detected on leptotene and zygotene stages (Figure 3A-B'; Movie S5; 176.3±36.1, n=10 nuclei), while pachytene nuclei present fewer and less bright DMC1 foci (Figure 3C, C'). In addition, we found that unlike in barley, we never observed nuclei with a polarized distribution of DMC1 foci. This highlights important differences in the spatiotemporal regulation of the early steps of meiotic recombination between barley and *Arabidopsis*, which could be at the origin of the strikingly different recombination patterns observed in these two species (Künzel *et al.*, 2000; Mayer *et al.*, 2012; Giraut *et al.*, 2011). We then investigated the localization of the ZMM protein HEI10 that is required for class I CO formation (Chelysheva *et al.*, 2012). HEI10 was shown to be present as numerous discrete foci at leptotene and zygotene (Chelysheva *et al.*, 2012). During pachytene the number of foci decreases, with the remaining brighter dots corresponding to class I COs that are retained until diakinesis (Chelysheva *et al.*, 2012). The HEI10 pattern we observed in intact meiocytes recapitulates the observations made on spread meiocytes (Chelysheva *et al.*, 2012). HEI10 is present at leptotene as numerous discrete foci and at early zygotene as bright foci and short stretches mostly on synapsed regions (Figure 3D-E'). As synapsis progresses HEI10 displays a linear and homogeneous pattern that colocalises with ZYP1 stretches (Figure 3F-H'). This SC central element associated HEI10 staining was already observed when HEI10 was detected on spread *A. thaliana* meiocytes, but only when mild spreading procedures (based on lipsol detergent) were applied (Chelysheva *et al.*, 2012). During pachytene, a subsequent number of cells displayed a very different signal with only few bright HEI10 foci and no central element labelling (Figure 3I, I'). This staining is likely to represent the progression of meiotic recombination toward the selection of mature COs, as shown in *A. thaliana* (Chelysheva *et al.*, 2012), rice (Wang *et al.*, 2012) and *S. macrospora* (De Muyt *et al.*, 2014). We also investigated the localization of MLH1 that marks class I COs from late pachytene until diakinesis (Chelysheva *et al.*, 2010). We found the same temporal and spatial localization pattern for MLH1 on intact meiocytes (Figure 3J-L'). Thus, a variety of antibodies to study the successive steps of meiotic recombination can be used on 3D preserved meiocytes.

A. thaliana meiocytes display a telomere bouquet

This technique that preserves the meiocytes 3D architecture gives us the opportunity to study their nuclear organization and the dynamics of specific chromosomal regions by performing *fluorescence in situ hybridization* (FISH). To investigate telomere behavior, we performed FISH with a probe that labels the repetitive telomeric sequences (Richards and Ausubel, 1988). The specificity of the signal was confirmed by three main observations. Firstly on pachytene nuclei where synapsed chromosomes are clearly distinguishable, the signal was seen on chromosome ends either as single dots or doublets (Figure S3A). Secondly, one or two bright foci were seen colocalising with a densely-stained DAPI centromere (Figure S3B, C). This observation is due to the presence of a telomere repeat sequences in the centromere of chromosome 1 (Richards *et al.*, 1991). Thirdly, the number of visible telomeric dots decreased as meiotic prophase I progressed as expected because of chromosome pairing (Figure S3D). We then analysed the telomere dynamics during prophase I. Previous studies on spread meiocytes showed that during premeiotic G2 telomeres localize at the nucleolus and during meiotic prophase I they are more likely associated with the nuclear periphery (Armstrong *et al.*, 2001; Varas *et al.*, 2015). We confirmed these observations since we found that during premeiotic G2 44.7% of the telomeric foci are nucleolus-associated (n=20 nuclei), 30.8% are at the nuclear periphery and the remaining
24.5% are both at the nuclear periphery and the nucleolus (Figure 4B, E). Indeed, during premeiotic G2 and meiotic prophase I the nucleolus is asymmetrically localized in the nucleus with one side being in close proximity to the nuclear periphery and the other side towards the center of the nucleus (Figure 4A). As meiocytes enter meiotic prophase I we found that almost all telomeres localize at the periphery of the nucleus and remain attached to the periphery until pachytene (Figure 4C, D, E; Movies S6, S7; leptotene/early zygotene 98.4% n=244 foci from 15 nuclei, zygotene 99% n=197 foci

from 15 nuclei, pachytene 99.4% n=164 foci from 15 nuclei). A fraction of the telomeric foci that localize at the nuclear periphery were also localized at the nucleolus (Figure 4C, D, E; Movies S6, S7). While G2 telomeres are scattered on the whole nucleolus and the nuclear periphery, the situation is very strikingly different when cells enter prophase I, since a clear clustering of telomere signals in a limited region of the nuclear periphery could be observed (Figure 5A), defining a clear bouquet. We observed that 47.7% and 40% of the meiocytes in leptotene (n=88) and zygotene (n=80) respectively displayed a telomere bouquet while 22.7% of the pachytene nuclei (n=75) analysed displayed a bouquet (Figure 5A, B and Movie S8). The ratio of telomeres in the bouquet reported to the total number of telomeres varies from 0.29 to 0.75 (Figure 5C) and we found no cases where all telomeres are part of the bouquet (leptotene n=42, zygotene n=32, pachytene n=17). We also observed different bouquet configurations. Indeed in some cases telomeres clustered in a very small volume; the lowest found being 6.67 μm^3 (Figure 5D, E). In other cases telomeres occupied a large volume on one side of the nucleus reminiscent to what was observed in *C. elegans* (Baudrimont *et al.*, 2010); the largest volume found being 145 μm^3 (Figure 5D, F). These findings raise questions as to whether the bouquet we observe in *A. thaliana* male meiocytes constitutes a modified version of the bouquet seen in large genome species where the bouquet is generally illustrated as a tight cluster where all or almost all telomeres participate (Cowan and Cande, 2002; Carlton *et al.*, 2003; Phillips *et al.*, 2010; Phillips *et al.*, 2012; Murphy *et al.*, 2014). The presence of nuclei with tight clustering of telomeres at the nuclear periphery suggests that whatever the functional significance of the bouquet, the telomere association at the nucleolus during G2 does not constitute a substitution for the tight bouquet organization during prophase I as previously suggested (Armstrong *et al.*, 2001). Indeed, the telomere arrangement we observe at the nucleolus in premeiotic G2 nuclei is not exclusive to meiotic cells. This organization was also seen in spread interphase nuclei of young flower buds, leaves, pollen mother cells and embryo-sac mother cells (Fransz *et al.*, 2002; Schubert *et al.*, 2012; Armstrong *et al.*, 2001). Thus, telomere association at the nucleolus during premeiotic G2 is likely to be a passive continuation of the organization observed in interphase cells. Put into the perspective of the above observation, that *Arabidopsis* SICs are close to the nuclear envelope where they tend to cluster at the leptotene/zygotene transition, the existence of a bouquet raises the possibility that the two events might be connected, which is reminiscent of what is known for plant species with large genomes (Golubovskaya *et al.*, 2011; Higgins *et al.*, 2012; Khoo *et al.*, 2012). In addition, it suggests that synapsis in *A. thaliana* initiates from the terminal regions of the chromosomes as it is the case for many organisms for which this question has been investigated, notably plants with large genomes (Zickler and Kleckner, 1998). This however was not expected to be the case of species such as *A. thaliana*, since, so far, terminally located SICs were always correlated with polarized recombination maps (Zickler and Kleckner, 1998). It has been known for a long time that recombination and synapsis are strongly connected, and that synapsis proceeds from sites of recombination (see discussion in (Chelysheva *et al.*, 2007)). In many organisms, and notably in plant species with large genomes, recombination events are principally located at the extremity of the chromosomes, leaving most of the proximal regions devoid of COs. This is however not the case in *A. thaliana* where the whole chromosome arms recombine (Giraut *et al.*, 2011). Thus, although chromosome organization in *A. thaliana* is different from large genome plant species (Künzel *et al.*, 2000; Roudier *et al.*, 2011; Mayer *et al.*, 2012; Choulet *et al.*, 2014; Giraut *et al.*, 2011), the meiotic processes of synapsis initiation and bouquet formation during prophase I seem to be well conserved and it is worth noting that recombination and synapsis initiation patterns can be uncoupled.

***A. thaliana* chromosomes are organized non-randomly in the nucleus**

We then compared the dynamics of two different subtelomeric regions, of the 3rd and 4th chromosomes respectively (Figure S4A). We checked that both probes displayed the expected pairing dynamics from premeiotic G2 to meiotic prophase I (Figure S4B and 6A-H) and that the signals emanating from both telomeric and subtelomeric probes always overlapped (Figure S4C, D). We then analyzed their nuclear localization during premeiotic G2 and prophase I. We found that during premeiotic G2 the majority of the subtelomeric regions of both chromosomes were at the nucleolus (chr3: 97.9% n=94, chr4: 81% n=58; Figure 6I, examples in Figure 6A & 6E). Upon entry into meiosis both the 3rd and 4th chromosome ends moved towards the nuclear periphery (from leptotene to

pachytene chr3: 94.7% n=264, chr4: 95% n=222) (Figure 6B-D, F-H, L and S5A-C). However, we noticed that the chromosome 3 subtelomeric region displayed an asymmetric localization pattern. Indeed, during premeiotic G2 very few foci were observed close to the nuclear periphery (7.6% n=92), revealing a preferential localization at the internal side of the nucleolus (Figure 6A, K, N). During meiotic prophase I however, most foci at the nuclear periphery were in the same nuclear hemisphere as the nucleolus suggesting that chromosome 3 end has a preferential nuclear territory (73.1% n=260, Figure 6M, N and S5D-F). We did not observe an asymmetric localization pattern for the subtelomeric region of chromosome 4 neither in G2 or prophase I (G2 40.4% close to the nuclear periphery, n=47; prophase I 56.8% same hemisphere as the nucleolus n=222) (Figure 6E, K, M, N and S5D-F). Thus our method for maintaining meiocytes intact allowed us to show for the first time that chromosome ends display different dynamics during premeiotic G2 and during the first stages of prophase I.

During the last few decades numerous studies in a wide range of species have led to a better understanding of how chromosomes are organized in the nuclear space (Cremer and Cremer, 2010; Tiang *et al.*, 2012; Rodriguez and Bjerling, 2013). For example it is now acknowledged that mammal and yeast interphase chromosomes occupy distinct territories in the nucleus (Cremer and Cremer, 2001; Sáez-Vásquez and Gadal, 2010). On the contrary, *A. thaliana* interphase chromosomes from flow sorted young root tips and rosette leaves visualized by whole chromosome painting display a random arrangement in the nuclear space (Pecinka *et al.*, 2004; Berr *et al.*, 2006). We have illustrated above that our technique for maintaining *A. thaliana* meiocytes intact gives the possibility to address these questions during the different stages of meiosis. Indeed, the behavior of other chromosomal ends and also other chromosomal regions such as centromeres should be addressed. Also whole chromosome painting would not only bring out information regarding the spatial arrangement of chromosomes along their entire lengths in the nuclear space but would also elucidate how chromosomes are organized during meiotic recombination and homolog pairing as it was so elegantly done in *C. elegans* (Nabeshima *et al.*, 2011).

CONCLUSIONS

A. thaliana has been a model of major importance for the study of meiosis during the past decades. Indeed, an important number of meiotic mutants were identified and together with advanced cytological and genetic approaches we now have a better understanding of various meiotic processes such as chromosome cohesion, meiotic recombination, synapsis, chromosome segregation and cell cycle regulation (Caryl *et al.*, 2003; Mercier *et al.*, 2015).

The cytological techniques used in various meiotic studies in *A. thaliana* consisted of performing immunolabeling or FISH spread meiocytes (Armstrong, 2013; Chelysheva *et al.*, 2013; Chelysheva *et al.*, 2010). Meiocyte spreading causes the loss of three-dimensional chromosome organization therefore limiting the extent to which nuclear dynamics can be studied. We set up a method for maintaining nuclear integrity in *A. thaliana* based on protocols used in large genome plant species. This method is fully compatible with immunohistochemistry since we showed that a variety of antibodies specific of different steps of meiosis can be used. 3D *Arabidopsis* meiocytes can also be used for FISH studies. This allowed us to characterize the telomere bouquet during meiotic prophase I and to illustrate differential behaviors of chromosomal subtelomeric regions during premeiotic G2 and prophase I. Our method opens new areas of research in the field of meiotic nuclear dynamics. The ability to maintain the nuclear organization of meiocyte nuclei in combination with the powerful cytogenetic tools of *A. thaliana* should help address the potential links between chromosome dynamics and other meiotic processes such as meiotic recombination, pairing and synapsis.

EXPERIMENTAL PROCEDURES

Plant material and growth conditions

A. thaliana Col-0 plants were grown in a greenhouse with a photoperiod of 16 h/day and 8 h/night, a temperature of 20˚C day and night and humidity 70%.

Extraction and polyacrylamide embedding of *A. thaliana* male meiocytes

To preserve their 3D architecture wild type Col-0 meiocytes were embedded in polyacrylamide as described below. Arabidopsis buds of 0.35-0.45 mm were isolated into Buffer A (80mM KCl, 20mM NaCl, 15mM Pipes-NaOH, 0.5mM EGTA, 2mM EDTA, 80mM Sorbitol, 1mM DTT, 0.15mM Spermine, 0.5mM Spermidine) and sepals and petals were removed to reveal the anthers. Buds were then fixed in 2% paraformaldehyde for 20-30 min followed by 2×10 minute washes in Buffer A. 10 µl of Buffer A was placed on a 22mm×22mm coverslip and 3-4 buds were deposited on the drop. The anthers were isolated in the drop with forceps and the rest of the buds were discarded. A 5 µl drop of activated 15% polyacrylamide solution (Buffer A/ 30% 29:1 acrylamide/bis acrylamide; to activate the polyacrylamide solution 2.5 µl of 20% sodium sulfite and 2.5 µl of 20% ammonium persulfate was added to a 50 µl polyacrylamide stock solution) was mixed to the Buffer A containing the anthers. A second coverslip was immediately deposited on the drop with a 45˚ angle relative to the first coverslip (Figure 1). Forceps were used to apply pressure on the embedded anthers to extract the meiocytes. The polyacrylamide gels were left to polymerize for at least 30 minutes. The two coverslips were then separated with a razor blade and the gel remains on one of the coverslips. A 5µl drop of distilled water was placed on a slide and the coverslip containing the gel pad was then placed on top, with the gel facing upwards. A drop of citifluor with DAPI (2µg/ml) is then added to the gel pad and a 22×40 mm coverslip placed on top. At this point slides can be either stored at 4˚C or processed directly for immunolabelling or FISH. We recommend screening the slides under an epifluorescence microscope beforehand to make sure gels have a sufficient number of meiocytes of the appropriate stages and to be certain that meiocyte nuclei architecture is not disrupted. Indeed, intact nuclei should be round with an appreciable z-depth at high magnification. Disrupted meiocyte nuclei due to excessive pressure during the preparation are not round anymore, look flat, sometimes parts of the chromatin are spreaded away from the rest of the DNA and at high magnification their zdepth is very small. Finally, if very little pressure is applied anthers are still intact and no or very few meiocytes are visible.

Immunolabelling of *A. thaliana* male meiocytes

Coverslips were removed from the slides and placed in a small Petri dish and are washed 3 x 10 min with PBS to remove citifluor. They are then washed with an excess of 1X PBS, 1% Triton X-100, 1 mM EDTA for 1h. Gel pads are then blocked with 2ml of blocking buffer (3% BSA in 1X PBS + 0.1% Tween 20) for at least two hours at room temperature. Blocking buffer is removed and 100 µl of primary antibody are deposited on the centre of the gel. The Petri dishes with gels are then placed into a humid chamber and incubated at room temperature for 1 hour before transferring at 4°C overnight. The next day the antibody is collected from the Petri dish, reapplied to the gel and incubated at room temperature for 1 hour. The solution is then removed and the gels are washed with PBS 4x30 min. 100 µl of the appropriate fluorophore conjugated secondary antibodies in blocking buffer are applied (1:100) to the gels and incubated at room temperature for 2 hours. The antibody solution is removed and gels are washed 3x10 minutes. Mounting is then performed like described above. Primary antibodies used are the following: rabbit α-DMC1 (1:20) (Vignard et al., 2007), rat α-ZYP (1:250) (Higgins et al., 2005), rabbit α-MLH1 (1:200) (Chelysheva et al., 2013), rabbit α-HEI10 (1:200) (Chelysheva et al., 2012). The guinea pig α-ASY1 (1:250) was produced in the following way: The coding region of the *A. thaliana* ASY1 gene was cloned into the protein expression vector pGEX-6P-1 (Amersham Pharmacia Biotech) as a N-terminal fusion to glutathione S-transferase (Armstrong et al., 2002). Upon induction, the GST-ASY1 fusion protein accumulated as insoluble inclusion bodies in E. coli BL21 cells. Purified, refolded recombinant protein was prepared as described previously (Chelysheva et al., 2010). Guinea pig polyclonal antiserum was produced against the GST-ASY1 fusion protein (Eurogentec).

FISH on *A. thaliana* male meiocytes

Coverslips are transferred to a small Petri dish and washed 3x 10 min with 2X SSC and are then transferred on slides. 100 µl of hybridization mix (50% deionized formamide, 2X SSC, 50 mM phosphate, pH 7.0, 10% dextran sulfate) containing the appropriate probes labelled with DIG or Biotin as described in (Chelysheva et al., 2008) [final concentration: 2ng/µl; BACS: pTAt4

(telomeres) (Richards and Ausubel, 1988), pAL1 (centromeres) (Martinez-Zapater et al., 1986), T4P13 and T5J17 (subtelomeric regions of chromosomes 3 and 4 respectively, TAIR accessions: 3601011 and 3601530 respectively)] was added on the gel pads and a 22x40 mm coverslip is placed on top. Gels are placed at 75°C for 8 min, and then transferred in a humid chamber and incubated at 37°C overnight. Coverslips with gels are transferred in small Petri dishes and washed briefly with 2X SSC followed by washes 2x30 min in 0.1X SSC; 20% formamide. Gels are then washed 2x30 min in 2X SSC at 37°C followed by two washes at room temperature. Gels are then blocked with 2 ml of blocking buffer (5% BSA in 4X SSC + 0.2% Tween 20) for at least two hours at room temperature. Blocking buffer is removed and the primary antibody mouse anti-DIG (1:100; Roche) and/or AvidinTexas Red (1:100; Vector laboratories) is applied on the gel and left to incubate for either two hours at room temperature or overnight at 4°C. Gels are then washed 3x15 minutes with 4X SSC + 0.2%
Tween 20 followed by 3x15 minute washes in PBS. Secondary antibodies rabbit anti-mouse Alexa488 (1:100; Molecular Probes) and/or goat anti-avidin-biotin antibodies (1:100; Vector laboratories) are then applied for two hours at room temperature followed by 3x15 minute washes in PBS. Finally, goat anti-rabbit Alexa-488 antibodies (1:100; Molecular Probes) and/or Avidin-Texas Red are applied for two hours at room temperature followed by a final 3x15 minute washes in PBS. Mounting is then performed like described above.

Image acquisition and processing
Observations were made using a Zeiss AxioImager 2 microscope. Photographs were taken using a Zeiss camera AxioCam MR driven by Axiovision 4.7 with a 60X/1.42 oil objective lens with 1.5X auxiliary magnification at 0.24 µm intervals along the z axis. All images were further processed with ImageJ FIJI. Selected images were deconvolved by first generating a theoretical point spread function (PSF) using the "diffraction PSF 3D" plugin (http://imagej.net/Diffraction_PSF_3D) followed by deconvolution using the "Iterative Deconvolve 3D" plugin (http://imagej.net/Iterative_Deconvolve_3D).

Data analysis
The volume of the telomere bouquet was measured by assimilating the bouquet as an ellipsoid and applying the equation $4/3\pi abc$. a, b, c being the lengths of the 3 axes in the bouquet volume were measured using ImageJ FIJI.
The proximity of subtelomeric foci at the nuclear periphery and the nucleolus was measured using ImageJ FIJI. Foci were considered as interacting with the nuclear periphery or the nucleolus when they were at a distance inferior to 0.5µm.

ACKNOWLEDGEMENTS
This work has benefited from a French State grant (LabEx Saclay Plant Sciences-SPS, ref. ANR-10LABX-0040-SPS), managed by the French National Research Agency under an "Investments for the Future" program (ref. ANR-11-IDEX-0003-02). The authors declare no conflicts of interest.

REFERENCES

Armstrong, S. (2013) Spreading and fluorescence in situ hybridization of male and female meiocyte chromosomes from *Arabidopsis thaliana* for cytogenetical analysis. *Methods Mol. Biol.*, 990, 3–11. Available at: http://www.ncbi.nlm.nih.gov/pubmed/23559197.

Armstrong, S.J., Caryl, A.P., Jones, G.H. and Franklin, F.C.H. (2002) Asy1, a protein required for meiotic chromosome synapsis, localizes to axis-associated chromatin in Arabidopsis and Brassica. *J. Cell Sci.*, 115, 3645–3655.

Armstrong, S.J., Franklin, F.C. and Jones, G.H. (2001) Nucleolus-associated telomere clustering and pairing precede meiotic chromosome synapsis in *Arabidopsis thaliana*. *J. Cell Sci.*, 114, 4207– 4217.

Barakate, A., Higgins, J.D., Vivera, S., et al. (2014) The synaptonemal complex protein ZYP1 is required for imposition of meiotic crossovers in barley. *Plant Cell*, 26, 729–740. Available at: http://www.pubmedcentral.nih.gov/articlerender.fcgi?artid=3967036&tool=pmcentrez&rendertype=abstract.

Baudrimont, A., Penkner, A., Woglar, A., et al. (2010) Leptotene/Zygotene chromosome movement via the SUN/KASH protein bridge in *Caenorhabditis elegans*. PLoS Genet., 6.

Berr, A., Pecinka, A., Meister, A., Kreth, G., Fuchs, J., Blattner, F.R., Lysak, M.A. and Schubert, I. (2006) Chromosome arrangement and nuclear architecture but not centromeric sequences are conserved between *Arabidopsis thaliana* and *Arabidopsis lyrata*. Plant J., 48, 771–783.

Carlton, P.M., Cowan, C.R. and Cande, W.Z. (2003) Directed motion of telomeres in the formation of the meiotic bouquet revealed by time course and simulation analysis. Mol. Biol. Cell, 14, 2832–43.

Caryl, A.P., Jones, G.H. and Franklin, F.C.H. (2003) Dissecting plant meiosis using *Arabidopsis thaliana* mutants. J. Exp. Bot., 54, 25–38.

Chelysheva, L.A., Grandont, L. and Grelon, M. (2013) Immunolocalization of meiotic proteins in *Brassicaceae*: method 1. Methods Mol. Biol., 990, 93–101. Available at: http://www.ncbi.nlm.nih.gov/pubmed/23559205.

Chelysheva, L., Gendrot, G., Vezon, D., Doutriaux, M.P., Mercier, R. and Grelon, M. (2007) Zip4/Spo22 is required for class I CO formation but not for synapsis completion in *Arabidopsis thaliana*. PLoS Genet., 3, 802–813.

Chelysheva, L., Grandont, L., Vrielynck, N., Guin, S. le, Mercier, R. and Grelon, M. (2010) An easy protocol for studying chromatin and recombination protein dynamics during *Arabidopsis thaliana* meiosis: immunodetection of cohesins, histones and MLH1. Cytogenet. Genome Res., 129, 143–53.

Chelysheva, L., Vezon, D., Belcram, K., Gendrot, G. and Grelon, M. (2008) The Arabidopsis BLAP75/Rmi1 homologue plays crucial roles in meiotic double-strand break repair. PLoS Genet., 4.

Chelysheva, L., Vezon, D., Chambon, A., et al. (2012) The Arabidopsis HEI10 is a new ZMM protein related to Zip3. PLoS Genet., 8.

Choulet, F., Alberti, A., Theil, S., et al. (2014) Structural and functional partitioning of bread wheat chromosome 3B. Science, 345, 1249721. Available at: http://www.sciencemag.org/content/345/6194/1250092.abstract.

Colas, I., Darrier, B., Arrieta, M., Mittmann, S.U., Ramsay, L., Sourdille, P. and Waugh, R. (2017) Observation of Extensive Chromosome Axis Remodeling during the "Diffuse-Phase" of Meiosis in Large Genome Cereals. Front. Plant Sci., 8, 1–9. Available at: http://journal.frontiersin.org/article/10.3389/fpls.2017.01235/full.

Cowan, C.R. and Cande, W.Z. (2002) Meiotic telomere clustering is inhibited by colchicine but does not require cytoplasmic microtubules. J. Cell Sci., 115, 3747–3756.

Cremer, T. and Cremer, C. (2001) Chromosome territories, nuclear architecture and gene regulation in mammalian cells. Nat. Rev. Genet., 2, 292–301. Available at: http://www.nature.com/nrg/journal/v2/n4/abs/nrg0401_292a.html%5Cnhttp://dx.doi.org/10.1038/35066075.

Cremer, T. and Cremer, M. (2010) Chromosome territories. Cold Spring Harb. Perspect. Biol., 2, a003889.

Fransz, P., Jong, J.H. de, Lysak, M., Castiglione, M.R. and Schubert, I. (2002) Interphase chromosomes in Arabidopsis are organized as well defined chromocenters from which euchromatin loops emanate. Proc. Natl. Acad. Sci., 99, 14584–14589. Available at: http://www.pnas.org/cgi/doi/10.1073/pnas.212325299.

Giraut, L., Falque, M., Drouaud, J., Pereira, L., Martin, O.C. and Mézard, C. (2011) Genome-wide crossover distribution in *Arabidopsis thaliana* meiosis reveals sex-specific patterns along chromosomes. PLoS Genet., 7.

Golubovskaya, I.N., Wang, C.J.R., Timofejeva, L. and Cande, W.Z. (2011) Maize meiotic mutants with improper or non-homologous synapsis due to problems in pairing or synaptonemal complex formation. J. Exp. Bot., 62, 1533–1544.

Higgins, J.D., Perry, R.M., Barakate, A., Ramsay, L., Waugh, R., Halpin, C., Armstrong, S.J. and Franklin, F.C.H. (2012) Spatiotemporal asymmetry of the meiotic program underlies the predominantly distal distribution of meiotic crossovers in barley. Plant Cell, 24, 4096–109. Available at: http://www.plantcell.org/content/24/10/4096.short.

Higgins, J.D., Sanchez-Moran, E., Armstrong, S.J., Jones, G.H. and Franklin, F.C.H. (2005) The Arabidopsis synaptonemal complex protein ZYP1 is required for chromosome synapsis and normal fidelity of crossing over. Genes Dev., 19, 2488–2500.

Khoo, K.H.P., Able, A.J. and Able, J. a (2012) The isolation and characterisation of the wheat molecular ZIPper I homologue, TaZYP1. BMC Res. Notes, 5, 106. Available at: http://www.pubmedcentral.nih.gov/articlerender.fcgi?artid=3305362&tool=pmcentrez&rendertype=abstract.

Klutstein, M. and Cooper, J.P. (2014) The chromosomal courtship dance-homolog pairing in early meiosis. Curr. Opin. Cell Biol., 26, 123–131. Available at: http://dx.doi.org/10.1016/j.ceb.2013.12.004.

Künzel, G., Korzun, L. and Meister, A. (2000) Cytologically integrated physical restriction fragment length polymorphism maps for the barley genome based on translocation breakpoints. Genetics, 154, 397–412. Available at: http://www.ncbi.nlm.nih.gov/pubmed/10628998.

Lee, C.Y., Conrad, M.N. and Dresser, M.E. (2012) Meiotic chromosome pairing is promoted by telomere-led chromosome movements independent of bouquet formation. PLoS Genet., 8.

Martínez-Pérez, E., Shaw, P., Reader, S., Aragón-Alcaide, L., Miller, T. and Moore, G. (1999) Homologous chromosome pairing in wheat. J. Cell Sci., 112 (Pt 1, 1761–1769.

Martinez-Zapater, J.M., Estelle, M.A. and Somerville, C.R. (1986) A highly repeated DNA sequence in Arabidopsis thaliana. MGG Mol. & Gen. Genet., 204, 417–423.

Mayer, K.F.X., Waugh, R., Langridge, P., et al. (2012) A physical, genetic and functional sequence assembly of the barley genome. Nature, 491, 711–716. Available at: http://dx.doi.org/10.1038/nature11543.

Mercier, R., Mézard, C., Jenczewski, E., Macaisne, N. and Grelon, M. (2015) The Molecular Biology of Meiosis in Plants. Annu. Rev. Plant Biol., 66, 297–327. Available at: http://www.annualreviews.org/doi/10.1146/annurev-arplant-050213-035923.

Murphy, S.P., Gumber, H.K., Mao, Y. and Bass, H.W. (2014) A dynamic meiotic SUN belt includes the zygotene-stage telomere bouquet and is disrupted in chromosome segregation mutants of maize (Zea mays L.). Front. Plant Sci., 5, 314.

Muyt, A. De, Zhang, L., Piolot, T., Kleckner, N., Espagne, E. and Zickler, D. (2014) E3 ligase Hei10: A multifaceted structure-based signaling molecule with roles within and beyond meiosis. Genes Dev., 28, 1111–1123.

Nabeshima, K., Mlynarczyk-Evans, S. and Villeneuve, A.M. (2011) Chromosome painting reveals asynaptic full alignment of homologs and him-8-dependent remodeling of x chromosome territories during *Caenorhabditis elegans* meiosis. PLoS Genet., 7.

Pecinka, A., Schubert, V., Meister, A., Kreth, G., Klatte, M., Lysak, M.A., Fuchs, J. and Schubert, I. (2004) Chromosome territory arrangement and homologous pairing in nuclei of *Arabidopsis thaliana* are predominantly random except for NOR-bearing chromosomes. Chromosoma, 113, 258–269.

Phillips, D., Nibau, C., Ramsay, L., Waugh, R. and Jenkins, G. (2010) Development of a molecular cytogenetic recombination assay for barley. Cytogenet. Genome Res., 129, 154–161.

Phillips, D., Nibau, C., Wnetrzak, J. and Jenkins, G. (2012) High resolution analysis of meiotic chromosome structure and behaviour in barley (Hordeum vulgare L.). PLoS One, 7.

Phillips, D., Wnetrzak, J., Nibau, C., Barakate, A., Ramsay, L., Wright, F., Higgins, J.D., Perry, R.M. and Jenkins, G. (2013) Quantitative high resolution mapping of HvMLH3 foci in barley pachytene nuclei reveals a strong distal bias. J. Exp. Bot., 64, 2139–2154.

Richards, E.J. and Ausubel, F.M. (1988) Isolation of a higher eukaryotic telomere from *Arabidopsis thaliana*. Cell, 53, 127–36. Available at: http://www.ncbi.nlm.nih.gov/pubmed/3349525.

Richards, E.J., Goodman, H.M. and Ausubel, F.M. (1991) The centromere region of *Arabidopsis thaliana* chromosome 1 contains telomere-similar sequences. Nucleic Acids Res., 19, 3351–7.

Roberts, N.Y., Osman, K. and Armstrong, S.J. (2009) Telomere distribution and dynamics in somatic and meiotic nuclei of *Arabidopsis thaliana*. Cytogenet. Genome Res., 124, 193–201.

Rodriguez, A. and Bjerling, P. (2013) The links between chromatin spatial organization and biological function. Biochem. Soc. Trans., 41, 1634–9.

Roudier, F., Ahmed, I., Bérard, C., et al. (2011) Integrative epigenomic mapping defines four main chromatin states in Arabidopsis. EMBO J., 30, 1928–1938.

Sáez-Vásquez, J. and Gadal, O. (2010) Genome organization and function: A view from yeast and Arabidopsis. Mol. Plant, 3, 678–690. Available at: http://dx.doi.org/10.1093/mp/ssq034.

Sato, S., Tabata, S., Hirakawa, H., et al. (2012) The tomato genome sequence provides insights into fleshy fruit evolution. Nature, 485, 635–641.

Scherthan, H. (2001) A bouquet makes ends meet. Nat. Rev. Mol. Cell Biol., 2, 621–627.

Schubert, V., Berr, A. and Meister, A. (2012) Interphase chromatin organisation in Arabidopsis nuclei: Constraints versus randomness. Chromosoma, 121, 369–387.

Tiang, C.-L., He, Y. and Pawlowski, W.P. (2012) Chromosome Organization and Dynamics during Interphase, Mitosis, and Meiosis in Plants. Plant Physiol., 158, 26–34. Available at: http://www.plantphysiol.org/cgi/doi/10.1104/pp.111.187161.

Varas, J., Graumann, K., Osman, K., Pradillo, M., Evans, D.E., Santos, J.L. and Armstrong, S.J. (2015) Absence of SUN1 and SUN2 proteins in *Arabidopsis thaliana* leads to a delay in meiotic progression and defects in synapsis and recombination. Plant J., 81, 329–346.

Vignard, J., Siwiec, T., Chelysheva, L., Vrielynck, N., Gonord, F., Armstrong, S.J., Schlögelhofer, P. and Mercier, R. (2007) The interplay of RecA-related proteins and the MND1-HOP2 complex during meiosis in *Arabidopsis thaliana*. PLoS Genet., 3, 1894–1906.

Wang, K., Wang, M., Tang, D., Shen, Y., Miao, C., Hu, Q., Lu, T. and Cheng, Z. (2012) The role of rice HEI10 in the formation of meiotic crossovers. PLoS Genet., 8.

Zheng, T., Nibau, C., Phillips, D.W., Jenkins, G., Armstrong, S.J. and Doonan, J.H. (2014) CDKG1 protein kinase is essential for synapsis and male meiosis at high ambient temperature in *Arabidopsis thaliana*. Proc. Natl. Acad. Sci., 111, 2182–2187. Available at: http://www.pnas.org/lookup/doi/10.1073/pnas.1318460111.

Zickler, D. (2006) From early homologue recognition to synaptonemal complex formation. Chromosoma, 115, 158–174.

Zickler, D. and Kleckner, N. (2016) A few of our favorite things: Pairing, the bouquet, crossover interference and evolution of meiosis. Semin. Cell Dev. Biol., 54, 135–148.

Zickler, D. and Kleckner, N. (1999) Meiotic chromosomes: integrating structure and function. Annu. Rev. Genet., 33, 603–754.

Zickler, D. and Kleckner, N. (2015) of Homologs during Meiosis. Cold Spring Harb. Lab. Press, 1,2.

Zickler, D. and Kleckner, N. (1998) The leptotene-zygotene transition of meiosis. Annu. Rev. Genet., 32, 619–697.

FIGURE LEGENDS

Figure 1. Procedure of *A. thaliana* male meiocyte isolation and maintenance. (A) Buds of the appropriate size are dissected and fixed in 2% PFA for 20-30 minutes in a glass dish. (B) Following two washes in buffer A 3-4 buds are transferred in a 10 µl drop of buffer A on a 22x22 mm coverslip and anthers are dissected out on the coverslip. (C) A 5 µl drop of 15% polyacrylamide is added and mixed by pipetting with the buffer A containing the anthers and another 22x22 mm coverslip is placed on top. (D) Gentle pressure is applied on the coverslip on top of each anther with fine forceps so as to extract the meiocytes and (E) and the polyacrylamide matrix is left to solidify for at least 30 minutes. (F) The two coverslips are then separated using a razor blade (G) and the coverslip with the polyacrylamide gel is placed in a small petri dish where it can be processed for immunohistochemistry or FISH (see Experimental procedures). (H) Eventually a drop of DAPI (2 µg/ml) is placed on top of the gel the coverslip is placed on top of a slide with the gel being between the slide and the coverslip and can be processed for imaging (see Experimental procedures).

Figure 2. Immunolocalisation of the synaptonemal complex proteins ASY1 (green) and ZYP1 (red) on intact male meiocytes. (A) ASY1 is present as puncta on decondensed chromatin during premeiotic G2 and ZYP1 is absent. (B) Upon entry into meiosis at leptotene chromatin condenses and is organized into fibers that are marked by ASY1. (C) The initiation of synapsis at the beginning of zygotene is revealed by the presence of ZYP1 (arrow). (D-F) Progression of zygotene is revealed by ZYP1 extension and reciprocal ASY1 removal (arrow in E). Unsynapsed chromatin still has ASY1 (arrowhead in E). (G) At pachytene chromosomes are synapsed as testified by the full extension of ZYP1 signal (n=34). An ASY1 focus can persist presumably at the rDNA locus (arrowhead). Figure S1 provides each single staining of ASY1 and ZYP1. All pictures correspond to projections of selected z-sections obtained by epifluorescence microscopy followed by deconvolution. Scale bars = 2

Figure 3. Immunolocalisation of the meiotic recombination proteins DMC1, HEI10 and MLH1 on intact male meiocytes. Numerous DMC1 foci are present on chromatin at leptotene (n=15 nuclei) (A-A') and zygotene (n=41) (B-B'). (C, C') DMC1 foci are present but faint at pachytene (n=41). (D, D') At leptotene HEI10 is present as numerous foci on unsynapsed chromosomes (n=21). (E, E') At early zygotene HEI10 is present as dots and short stretches on synapsed chromosomes (n=19). (F, F') As synapsis progresses HEI10 becomes homogeneously present on synapsed chromosomes (n=72). (G-I') Different localization patterns of HEI10 during pachytene: HEI10 can form homogenous (GG', n=50) or patchy (H-H', n=36) signals on the central element of the SC (arrowheads in H' point to locations where HEI10 is strongly present). (I-I') At late pachytene HEI10 forms a few bright corresponding to class I CO sites (n=24). (J-L') MLH1 forms a few bright foci at pachytene (J, J', n=50), diplotene (K, K', n=102), and diakinesis (L, L', n=37). All pictures correspond to projections of selected z-sections and were obtained by epifluorescence microscopy followed by deconvolution. Scale bars = 2 µm

Figure 4. Telomere localization during premeiotic G2 and meiotic prophase I. (A) Schematic representation representing the nuclear localization of the nucleolus during premeiotic G2 and meiotic prophase I. (B-D) FISH on intact Col-0 male meiocytes with telomeric probe pTat4. All pictures correspond to projections of selected z-sections and were obtained by epifluorescence microscopy followed by deconvolution. During premeiotic G2 (B) telomeres can be found at the nucleolus (arrows) at the nuclear periphery (arrowhead) or at both compartments. During zygotene (C) and pachytene (D) telomeres localize mostly at the nuclear periphery (arrows) (n = nucleolus). (E) Quantification of the proportions of telomere foci localizing at the nuclear periphery, the nucleolus, at both compartments and at none of the two compartments from premeiotic G2 to pachytene (premeiotic G2: n=409 foci from 20 nuclei; leptotene/early zygotene: n=244 foci from 15 nuclei; zygotene: n=197 foci from 15 nuclei; pachytene: n=164 foci from 15 nuclei). Scale bars = 2 µm

Figure 5. *A. thaliana* male meiocytes display a telomere bouquet. (A, E, F) FISH on intact Col-0 male meiocytes with telomeric probe pTat4. All pictures correspond to projections of selected zsections and were obtained by epifluorescence microscopy followed by deconvolution. (A) Example of a meiocytes showing a telomere bouquet (dashed ellipse). (B) Quantification of the proportion of meiocytes displaying a telomere bouquet from premeiotic G2 to pachyte ne (premeiotic G2: n=76; leptotene/early zygotene: n=88; zygotene: n=80; pachytene: n=75). (C) Quantification from randomly selected nuclei from all stages of the ratio number of telomere foci in a bouquet/total number of telomeric foci in a nucleus (0.5±0.12; n=24). (D) Quantification from randomly selected nuclei from all stages of the volume of the bouquet (V=43.5±39 µm3; n=24). (E, F) Representative examples of a very small bouquet and a very large one (see dashed ellipses). Scale bars = 2 µm

Figure 6. Dynamics of individual chromosomal ends. (A-H) FISH on intact Col-0 male meiocytes with subtelomeric probes T4P13 (IIIrd chromosome, A-D) and T5J17 (IVth chromosome, E-H). All pictures correspond to projections of selected z-sections and were obtained by epifluorescence microscopy followed by deconvolution. (A, E) Example of nucleolus-association of subtelomeric regions of chromosomes 3 (A) or 4 (E) during premeiotic G2. (B-D) Examples displaying the nonrandom localization of the subtelomeric regions of chromosomes 3 at the nuclear periphery. (F-H) Examples displaying the random localization of the subtelomeric regions of chromosomes 4 at the nuclear periphery. Quantifications of the percentage of subtelomeric foci at the nucleolus (I) and at the nuclear membrane (J) during premeiotic G2. (K) Quantification of the percentage of subtelomeric foci localized at the nucleolus that are in close proximity to the nuclear membrane during premeiotic G2. (L) Quantification of the percentage of subtelomeric foci at the nuclear membrane during prophase I. (M) Quantification of the percentage of subtelomeric foci localized in the same hemisphere as the nucleolus during prophase I. (N) Diagram illustrating how subtelomeric regions of chromosomes 3 and 4 are distributed during premeiotic G2 and prophase I. In all pictures n = nucleolus. Scale bars = 2 µm

Figure 1

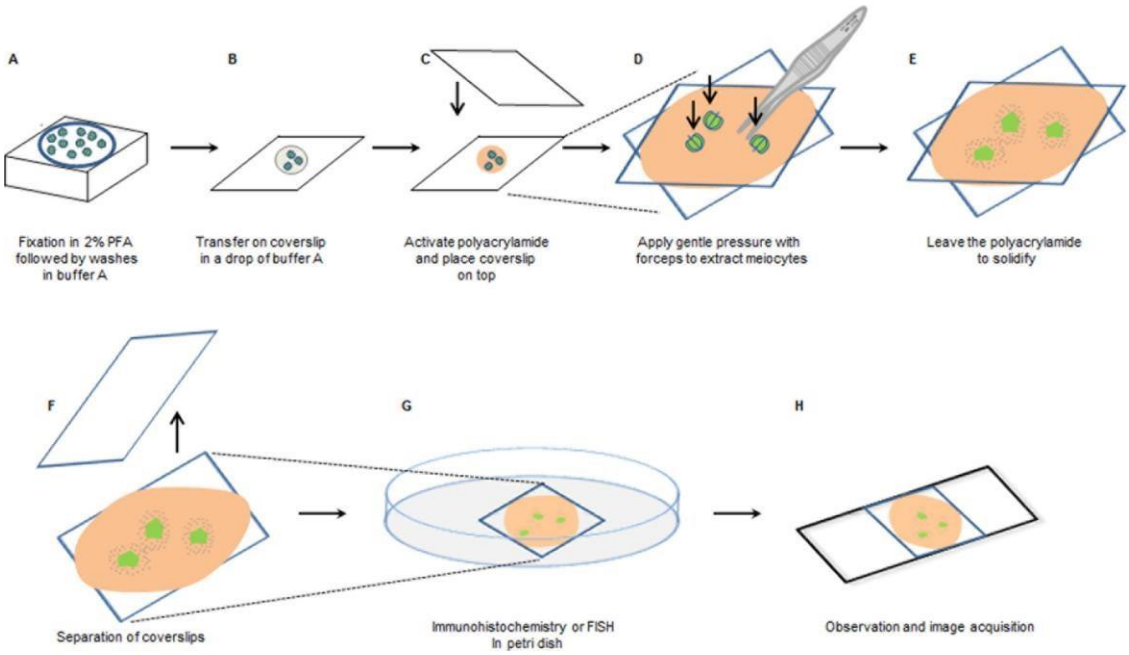
A
B
C
D
E
Fixation in 2% PFA followed by washes in buffer A
Transfer on coverslip in a drop of buffer A
Activate polyacrylamide and place coverslip on top
Apply gentle pressure with forceps to extract meiocytes
Leave the polyacrylamide to solidify
F
G
H
Separation of coverslips
Immunohistochemistry or FISH in petri dish
Observation and image acquisition

Figure 2

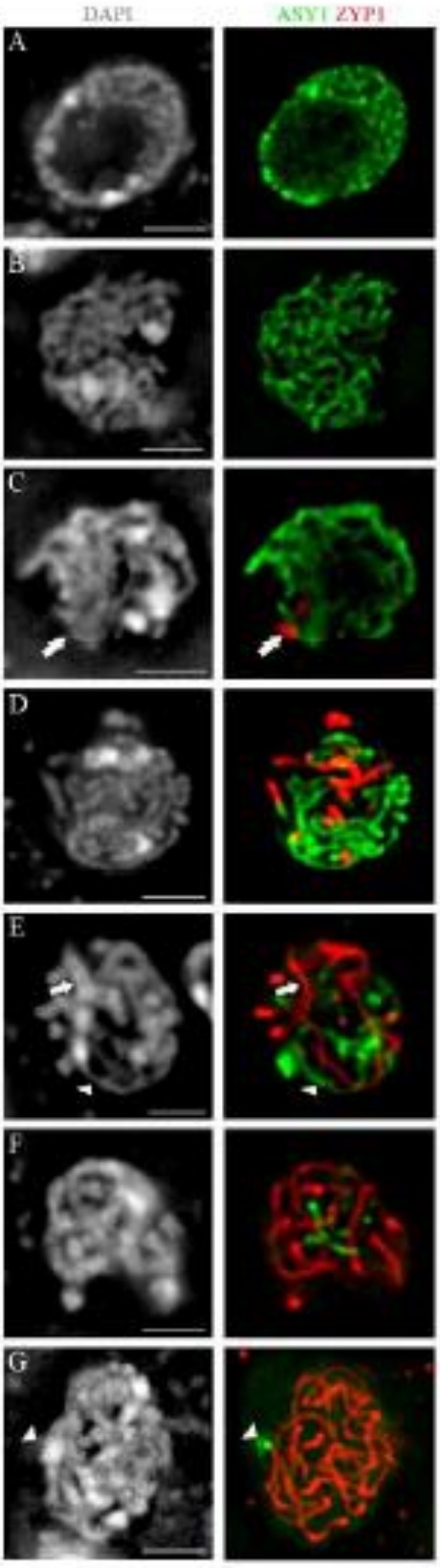

Figure 3

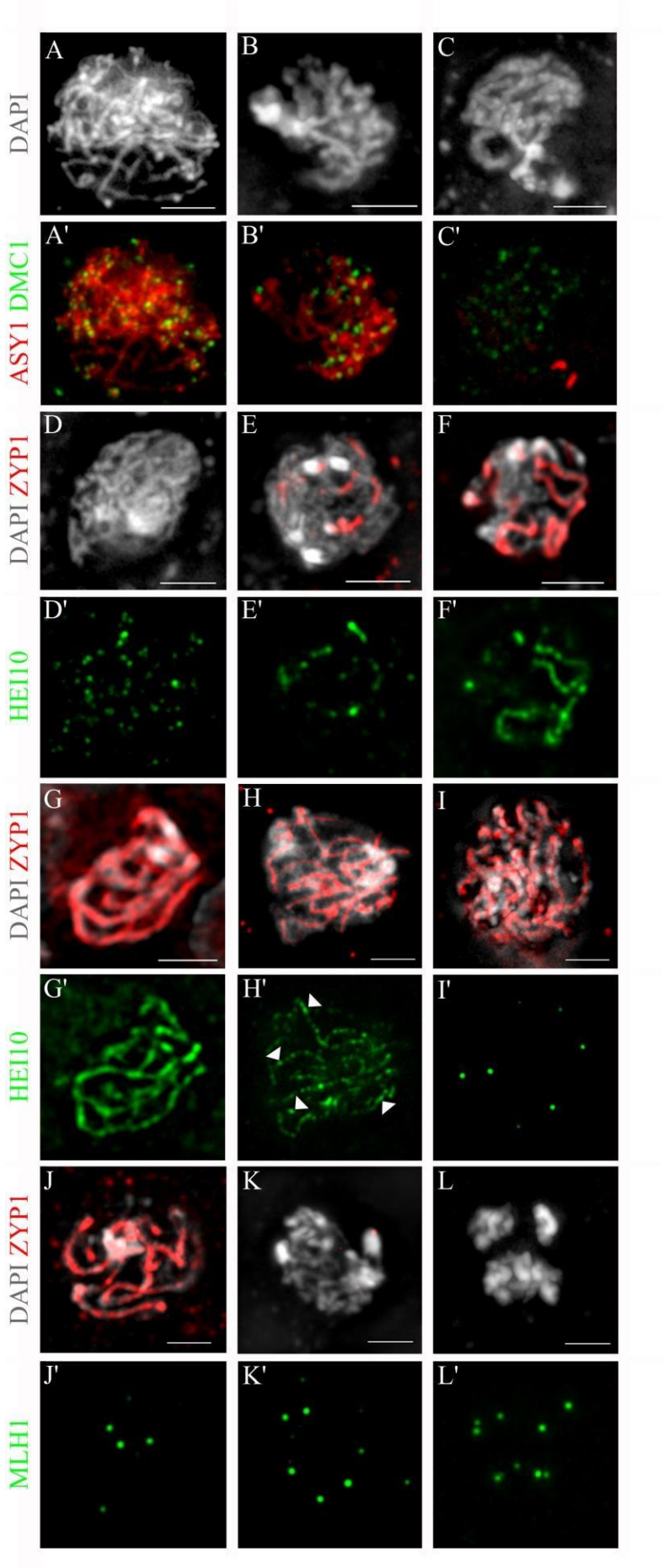
DAPI
A
B
C
ASY1 DMC1
A'
B'
C'
DAPI ZYP1
D
E
F
HEI10
D'
E'
F'
DAPI ZYP1
G
H
I
HEI10
G'
H'
I'
DAPI ZYP1
J
K
L
MLH1
J'
K'
L'

Figure 4

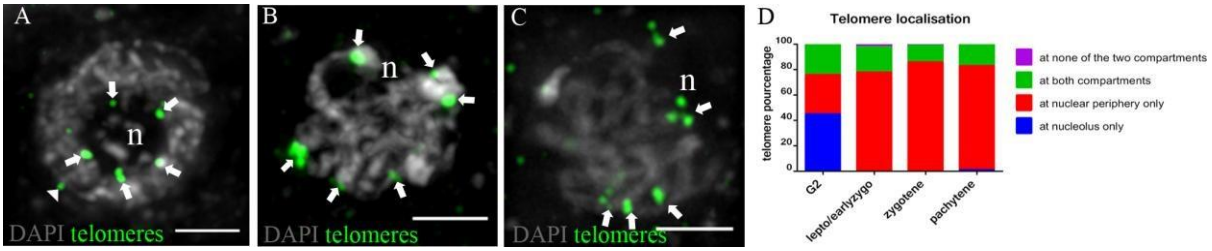

Figure 5

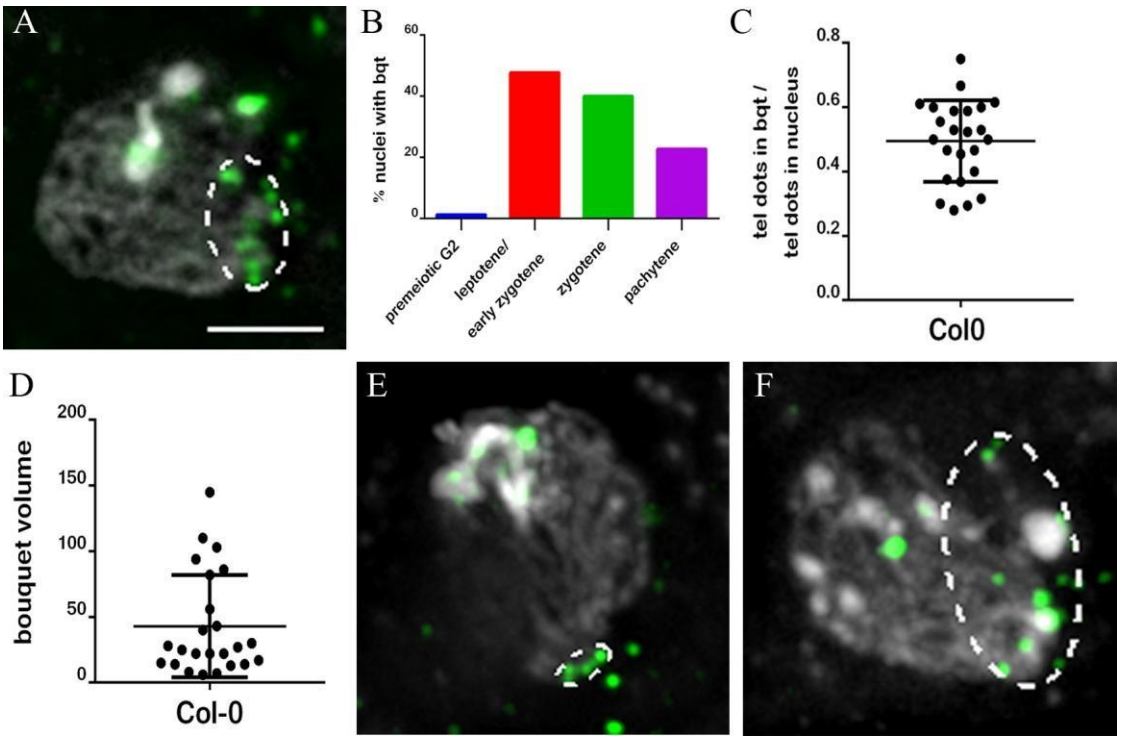

Figure 6

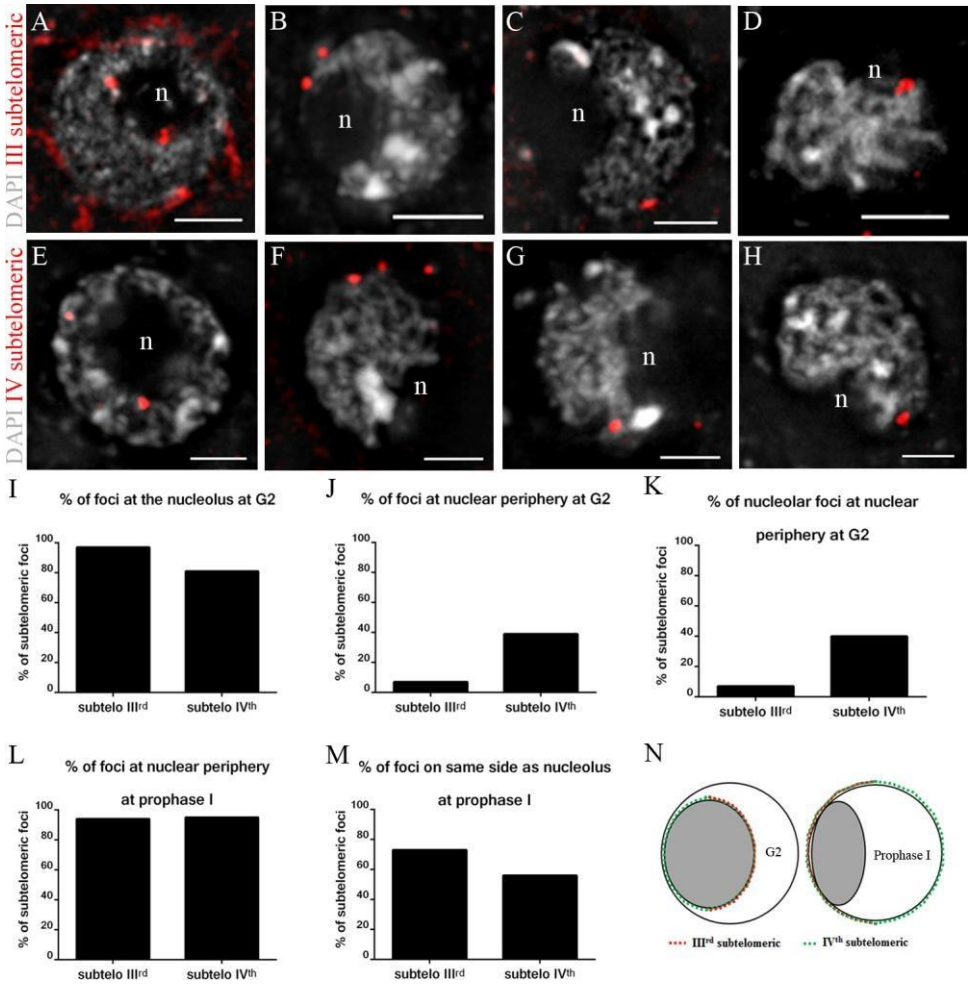
DAPI III subtelomeric
DAPI IV subtelomeric
A
B
C
D
E
F
G
H
n
I
% of foci at the nucleolus at G2
J
% of foci at nuclear periphery at G2
K
% of nucleolar foci at nuclear periphery at G2
% of subtelomeric foci
subtelo IIIrd
subtelo IVth
L
% of foci at nuclear periphery at prophase I
M
% of foci on same side as nucleolus at prophase I
N
G2
Prophase I
IIIrd subtelomeric
IVth subtelomeric